Lanthanide Luminescence Thermometry and Slow Magnetic Relaxation in 3-D Polycyanidometallate-Based Materials

Konstantinos Karachousos-Spiliotakopoulos, Vassilis Tangoulis,* Nikos Panagiotou, Anastasios Tasiopoulos, Vassilis Nastopoulos, Eufemio Moreno-Pineda,* Wolfgang Wernsdorfer,* Michael Schulze, Alexandre M. P. Botas, and Luis D. Carlos*

ABSTRACT: Two three-dimensional (3-D) polycyanidometallate-based luminescent thermometers with the general formula $\{Ln_4Co_4(CN)_{24}(4\text{-benpyo})_{17}(H_2O)\cdot 7H_2O\}_n$ Ln = (Dy(III)(**1**), Eu(III)(**2**)), based on the red-emissive diamagnetic linker $[Co(CN)_6]^{3-}$ and the bulky pyridine derivative that possesses the N-oxide moiety, 4-benzyloxy-pyridine N-oxide (benpyo), were prepared for the first time. The structure of compound **1** has been determined by single-crystal X-ray crystallography while the purity and structure of **2** have been confirmed by CHN, Fourier transform infrared spectroscopy (FT-IR), and powder X-ray diffraction (PXRD) analysis. Magnetic AC susceptibility measurements at zero field show no single-molecule magnet (SMM) behavior indicating fast relaxation operating in **1**. Upon application of an optimal field of 2 kOe, the SMM character of compound **1** is revealed while the $\tau(T)$ can be reproduced solely considering the Raman process $\tau^{-1} = CT^n$ with $C = 7.0901(3)$ s^{-1} K^{-n} and $n = 3.58(1)$, indicating that a high density of low-lying states and optical as well as acoustic phonons play a major role in the relaxation mechanism. Micron-sized superconducting quantum interference device (μ-SQUID) loops show a very narrow opening in agreement with the AC susceptibility studies and complete active space self-consistent field (CASSCF) calculations. The interaction operating between the Dy(III) ions was quantified from CASSCF calculations. Good agreement is found by fitting the experimental DC $\chi_M T(T)$ and $M(H)$, employing the Lines model, with $J_{Lines} = -0.087$ cm^{-1} (−0.125 K). The excitation spectra of compound **2** are used for temperature sensing in the 25−325 nm range with a maximum relative thermal sensitivity, $S_r = 0.6\%$ K^{-1} at 325 K, whereas compound **1** operates as a luminescent thermometer based on its emission features in the temperature range of 16−350 K with $S_r \approx 2.3\%$ K^{-1} at 240 K.

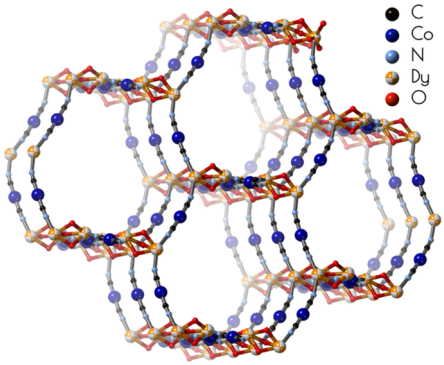

INTRODUCTION

A new generation of light-emitting materials that act as remote thermometer sensors appeared in the middle of the last decade due to the need to replace conventional contact-type thermometers that failed in their role in monitoring the temperature at micro and nanoscales (for instance, during the operation of spintronic devices).[1,2] Consequently, the need to combine two different physical properties into a single-phase material led to multifunctional materials[3−6] that could monitor cooperative effects or the effect of one property on the other.[3,7] It should be noted here that the range of possible applications of these materials can be expanded if these physical properties are uncoupled, introducing a multitasking mode under the same operational conditions.

Multifunctionality in the field of molecular materials, combining magnetic and optical properties, is a promising research path due to the need to create smart devices based on properties that are induced at the molecular level. The use of trivalent lanthanide ions is a recipe for success as they are widely used for the synthesis of molecular magnetic materials called single-molecule magnets (SMMs). These are molecular materials exhibiting strong magnetic anisotropy, accompanied by a magnetic hysteresis loop of a molecular origin.[8,9] The magnetic characteristics of SMMs make them prospective candidates for the field of spintronics, as well as for data storage applications.[10] On the other hand, trivalent lanthanide ions are known for their emission properties due to f−f transitions that can be observed over the whole range of electromagnetic spectrum from the UV (Gd^{3+}), to the visible (e.g., Tb^{III}, Dy^{III}, Eu^{III}), to the NIR (e.g., Nd^{III}, Yb^{III}, Er^{III}).[11] Such a wide range of emissions offers a wide range of possible applications such as display devices, optical storage, sensing, and bioimaging.[12,13] The combination of optical characteristics and the slow relaxation of the magnetization of lanthanides has recently become a new area of research where (a) molecular

photoluminescent thermometers can act as an efficient tool to detect the temperature at the nanoscale[14,15] and (b) the correlation of the thermally activated mechanisms of magnetization with the luminescence properties of lanthanide ions is thoroughly investigated.[16]

White-light-emitting or multicolored/NIR-emissive nanomagnets have quickly started to appear in the literature,[17−22] and correlations have begun to be reported concerning the SMM character and luminescence since both phenomena are related to the electronic structure of 4f-metal ions.[23−26] The main interest of the scientific community is in the optical determination of the anisotropic energy barrier, ΔE, from the high-resolution emission spectra at low temperatures. It should be noted that another exciting property of SMM luminescence thermometers is the so-called optomagnetic sensitivity according to which their properties are conserved under the application of an external magnetic field.[7,27−30]

We have decided to explore the combination of (a) the magnetically anisotropic and emissive Dy^{III} ion with (b) the red-emissive diamagnetic units and (c) bulky pyridine derivatives that possess N-oxide moieties,[31] as a promising source for effective energy transfer to the lanthanide ion, as well as effective separators of the paramagnetic Dy^{III} centers. The reason for this quest is the limited number of compounds that appeared in the literature so far which are only low-dimensional Dy^{III}-$[Co(CN)_6]^{3-}$ materials[18,32−35] with no related 3-D frameworks, except the 3-D complex $\{Dy(H_2O)_2[Co(CN)_6]\}\cdot 2H_2O$.[36] This list can be further narrowed down to only two compounds experimentally verified as polycyanidometallate-based SMM luminescent thermometers. The heterodinuclear 3d−4f compound, $[Dy-Co^{III}(CN)_6(bpyO_2)_2\ (H_2O)_3]\cdot 4H_2O$ ($bpyO_2$ = 2,2′-bipyridine-*N*,*N*′-dioxide) (reported by our group)[33] exhibiting S_r = 1.84% K^{-1} at 70 K in the temperature range of 40−140 K, and the 2-D cyanido-bridged layers of $\{[Tb_xDy_{1-x}(4-OHpy)_2(H_2O)_3][Co^{III}(CN)_6]\}$ where 4-OHpy = 4-hydroxypyridine[15] and x = 1.0, 0.5 with S_r >1% K^{-1} in the 120−200 K temperature range. While in the first case the diamagnetic linker $[Co(CN)_6]^{3-}$ serves as a "bulky separator" of magnetically anisotropic lanthanide compounds, in the second case it plays the role of a diamagnetic linker between the lanthanide ions altering the SMM characteristics of the compound. Herein, we report (for the first time) the synthesis of 3-D polycyanidometallate-based SMM luminescent thermometers employing the trivalent lanthanide ions, Dy^{III} and Eu^{III}, with the diamagnetic linker $[Co(CN)_6]^{3-}$ and the bulky pyridine derivative 4-benzyloxy-pyridine N-oxide (benpyo).

EXPERIMENTAL SECTION

Materials, Physical Techniques, and Spectroscopic Methods. All manipulations were performed under aerobic conditions using materials ($DyCl_3\cdot 6H_2O$, 4-benpyo, $K_3[Co(CN)_6]$) as received. H_2O was distilled in-house. Elemental analyses (C, H, N) were performed by the Laboratory of Instrumental Analysis at the University of Patras. FT-IR spectra (4000−400 cm^{-1}) were recorded using a Perkin-Elmer 16PC spectrometer; the samples were in the form of KBr pellets.

Magnetic Measurements. The DC magnetic susceptibility measurements for **1** were performed using the magnetometers Quantum Design MPMS 3 and MPMS-XL SQUID on crystals that were carefully powdered. The temperature range of the measurements was 2−300 K under an external magnetic field of 1 kOe. AC magnetic measurements were collected using an oscillating magnetic field of 3.5 Oe and frequencies between 1 and 1.5 kHz while an external DC magnetic field was applied in the range 0−5 kOe. Diamagnetic contributions from the eicosane and core diamagnetism were corrected employing Pascal's constants. Single-crystal magnetization measurements were carried out in the temperature range of 0.03−2 K using a μ-SQUID apparatus at sweep rates between 0.002 and 0.280 T s^{-1} while the resolution of time was ∼1 ms. To apply the magnetic field in any direction of the μ-SQUID plane, three orthogonal coils were driven separately. For the μ-SQUID magnetization measurements, the transverse field method was employed according to which the magnetic field was applied parallel to the easy axis of magnetization.

Optical Measurements. The photoluminescence spectra were recorded using a modular double-grating excitation spectrofluorometer with a TRIAX 320 emission monochromator (Fluorolog-3, Horiba Scientific) coupled to a R928 Hamamatsu photomultiplier, using a front-face acquisition mode. The excitation source was a 450 W Xe arc lamp. The emission spectra were corrected for detection and optical spectral response of the spectrofluorometer, and the excitation spectra were corrected for the spectral distribution of the lamp intensity using a photodiode reference detector. The temperature was varied using a helium closed-cycle cryostat, a vacuum system (4×10^{-4} Pa), and an autotuning temperature controller (Lakeshore 330, Lakeshore) with a resistance heater. To ensure the complete thermalization of the samples, all of the measurements were initiated 300 s after the temperature was stabilized according to the indication of the temperature controller.

Preparation of $\{[Dy_4Co_4(CN)_{24}(4\text{-benpyo})_{17}(H_2O)]\cdot 7H_2O\}_n$ ***(1)***. A solution of $K_3[Co(CN)_6]$ (23.0 mg, 0.07 mmol) in H_2O (1.1 mL) was rapidly added to a stirred warm solution containing $DyCl_3\cdot 6H_2O$ (26.0 mg, 0.07 mmol) and 4-benpyo (14.0 mg, 0.07 mmol) in H_2O (1.1 mL). The resulting pale yellow solution was shaken by hand to become homogeneous and stored in a closed vial at room temperature. X-ray quality, pale yellow crystals of compound **1** were grown in a period of 1 day. The crystals were collected by filtration, washed with EtOH (2 × 0.5 mL) and Et_2O (3 × 1 mL), and dried in air. The yield was ∼75% (based on the organic ligand used). Anal. Calcd. for $C_{228}H_{203}N_{41}O_{42}Dy_4Co_4$: C 53.96; H 4.04; N 11.32%. Found: C 54.01; H 3.70; N 11.20%. IR (KBr, cm^{-1}): 3394mb, 3124m, 3060w, 2905w, 2124s, 1630s, 1572m, 1498s, 1454m, 1388m, 1298s, 1220sb, 1106w, 1080sh, 984s, 920w, 842s, 794s, 746m, 696s; 614w, 562w, 514m, 416w.

Preparation of $\{[Eu_4Co_4(CN)_{24}(4\text{-benpyo})_{17}(H_2O)]\cdot 7H_2O\}_n$ ***(2)***. A solution of $K_3[Co(CN)_6]$ (23.0 mg, 0.07 mmol) in H_2O (1.1 mL) was rapidly added to a stirred warm solution containing $EuCl_3\cdot 6H_2O$ (25.6 mg, 0.07 mmol) and 4-benpyo (14.0 mg, 0.07 mmol) in H_2O (1.1 mL). The resulting pale yellow solution was shaken by hand to become homogeneous and stored in a closed vial at room temperature. Fragile and poor X-ray quality, pale yellow crystals of compound **2** were grown in a period of 1 day. The crystals were collected by filtration, washed with EtOH (2 × 0.5 mL) and Et_2O (3 × 1 mL), and dried in air. The yield was ∼75% (based on the organic ligand). The purity and the structure of compound **2** have been confirmed by CHN, FT-IR, and PXRD analysis (Figures S1 and S2). Anal. Calcd. for $C_{228}H_{203}N_{41}O_{42}Eu_4Co_4$: C 54.41; H 4.07; N 11.41%. Found: C 54.61; H 3.87; N 11.26%. IR (KBr, cm^{-1}): 3394mb, 3124m, 3060w, 2905w, 2124s, 1630s, 1572m, 1498s, 1454m, 1388m, 1298s, 1220sb, 1106w, 1080sh, 984s, 920w, 842s, 794s, 746m, 696s; 614w, 562w, 515m, 425w, 415m, 407w.

Single-Crystal X-ray Crystallography. A suitable single crystal of compound **1**, covered with paratone-N oil, was scooped up in a cryo-loop and transferred to a cryostat, where it was cooled under a flow of nitrogen gas at 108(2) K. Diffraction data were collected (ω-scans) on a SuperNova diffractometer constructed by Rigaku using Cu Kα radiation (λ = 1.5418 Å). Data were collected and processed using CrysAlis CCD and RED software,[37] respectively. The reflection intensities were corrected for absorption by the multiscan method. The structure was solved using direct methods with SIR92[38] and refined by full-matrix least-squares on F^2 with SHELXL-2014/7.[39] Anisotropic refinement was applied for all non-H atoms. There is a significant disorder in the structure which mainly affects the phenyl

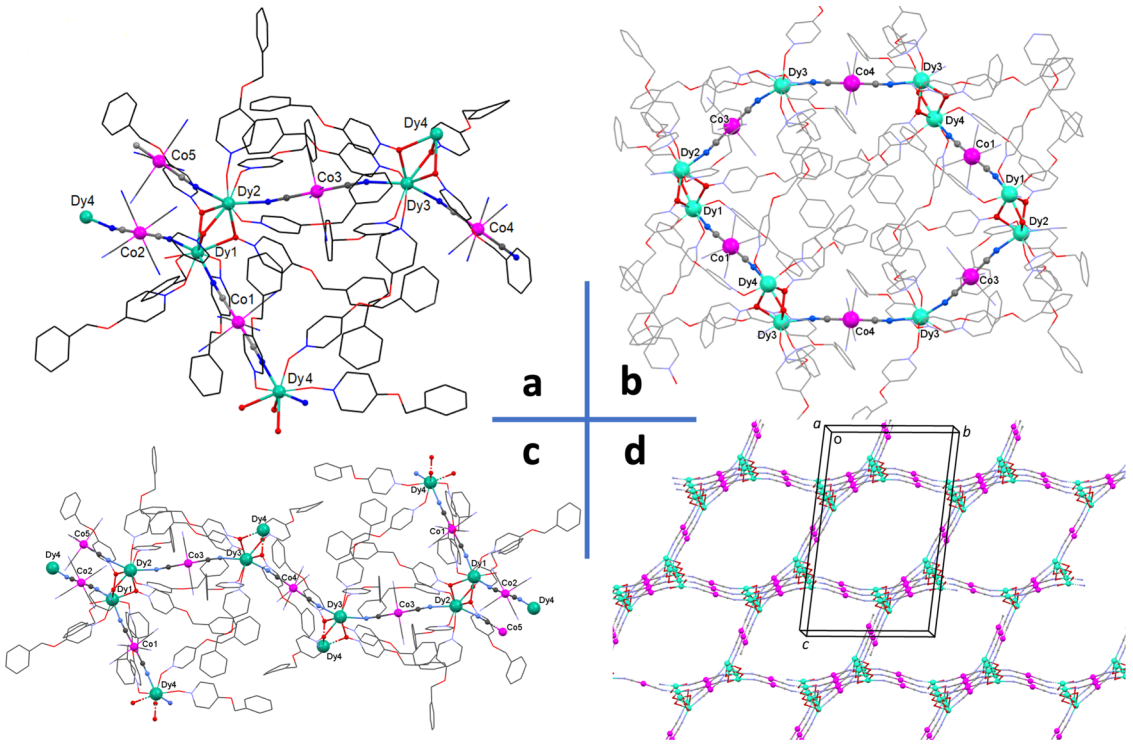

Figure 1. (a) Partially labeled view of the asymmetric unit of the 3-D polymeric compound **1**. (b) One of the six rings (with different metal sequences) that are present in the crystal structure of the 3-D polymeric compound **1**. (c) Part of the 3-D structure of **1** showing the propagation of the polymeric structure. (d) A view of the 3-D polymeric structure of compound **1** down axis a showing five complete rings. Only the atoms participating in the rings have been drawn. The color code is the same in the four subfigures: Dy, light green; O, red; C, gray; N, blue; and Co, pink.

rings of the 4-benpyo ligands, five of which have been modeled over two orientations. Care was taken during refinement, using appropriate restraints and constraints, to be consistent with the geometry of the disordered groups. Carbon-bound H atoms were included at calculated positions and allowed to ride on their carrier atoms (riding model). Due to the disorder and the presence of heavy metal ions, the H atoms of the coordinated (O35) and lattice (O36−O43) H_2O molecules could not be reliably located in difference Fourier maps; therefore, these H atoms have not been included in the structural model. The crystal structure also contains a small area of highly disordered solvent (~5 H_2O molecules/unit cell). For this reason, the SQUEEZE[40] function of PLATON[41] was employed to remove the contribution of the electron density associated with those solvent molecules from the intensity data. The solvent-free model and intensity data were used for the final reported results. Geometric/crystallographic calculations were carried out using WINGX[42] and PLATON[41] packages. Molecular/packing graphics were prepared by DIAMOND[43] and MERCURY.[44] Experimental details are listed in Table S1.

RESULTS AND DISCUSSION

Synthetic Comments and IR Spectra. Concerning the reaction system $Dy^{III}/K_3[Co^{III}(CN)_6]$/4-benpyo, several crystallization methods were employed using various reagent ratios and solvent media. The optimized conditions involve the 1:1:1 reaction of $DyCl_3{\cdot}6H_2O$, $K_3[Co(CN)_6]$, and 4-benpyo in slightly warm H_2O leading to a pale yellow solution from which yellowish crystals of **1** were subsequently isolated in a very good yield. The formation of the compound is summarized in eq 1. The reaction conditions yield a high yield but simultaneously keeps the KCl by-product soluble; thus, the compound can be analytically pure. The 1:1:2 and 2:2:1 Dy^{III}/Co^{III}/4-benpyo reaction ratios in H_2O were also tested. The former yielded a crystalline precipitate of **1** (analytical and IR evidence), while the latter had as a result the growth of yellow crystals whose IR spectrum was different from that of **1** suggesting a different product; the crystals were repeatedly of poor quality, and therefore, the structure of the second product remains unknown to date.

$$4nDyCl_3{\cdot}6H_2O + 4nK_3[Co(CN)_6] + 17n4 - benpyo \rightarrow \{[Dy_4Co_4(CN)_{24}(4 - benpyo)_{17}(H_2O)]{\cdot}7H_2O\}_n + 12nKCl + 16nH_2O\,\mathbf{1} \quad (1)$$

In Figure S1 is shown the IR spectrum of compound **1**. The medium-intensity bands at ~3400 and ~3130 cm^{-1} are assigned to the stretching O−H vibration [ν(OH)] of the lattice and coordinated H_2O, respectively.[45] The higher-wavenumber band is broad, suggesting strong hydrogen-bonding interactions. The strong band at 1630 cm^{-1} is correlated to the δ(OH) vibration of water molecules, probably involving also a stretching aromatic character (the spectrum of free, i.e., uncoordinated, 4-benpyo exhibits a weak band at 1624 cm^{-1}). The stretching vibrations of the pyridine-N oxide and phenyl rings of coordinated 4-benpyo[46] bands of compound **1** are depicted in the range of 1630−1388 cm^{-1}, slightly shifted in comparison to the free 4-benpyo. The ν(N−O) vibration[46] in the spectrum of compound **1** is assigned at 1220 cm^{-1} (strong band) considerably shifted in comparison to the free ligand (1274 cm^{-1}) due to the coordination of the ligand. The ν(C≡N) mode of the bridging cyanido groups[47] of compound **1** is located in a strong band at 2124 cm^{-1}.

Description of Structure. The crystal structure of **1** was determined by single-crystal X-ray crystallography and is

shown in Figure 1 with four different orientations while several selected interatomic distances are listed in Table S2.

Compound **1** crystallizes in the triclinic space group $P\bar{1}$. It is a 3-D coordination polymer consisting of rings that contain 16 metal ions; 10 are Dy^{III} centers and six are Co^{III} ions. The asymmetric unit comprises four Dy^{III} ions and four Co^{III} ions (Figure 1a,c). Co4 and Co5 have half occupancy, each lying on an inversion center. There are six rings in the lattice, each of them containing different metal arrangements. For example, the ring shown in Figure 1b (which contains all of the ligands) has the sequence Co1Dy1Dy2Co3Dy3Co4Dy3Dy4 Co1Dy1-Dy2Co3Dy3Co4Dy3Dy4. The rings share common edges creating the 3-D architecture (Figure 1d).

Two of the cyanido groups act as bridging ligands, linking each Co^{III} center with two neighboring Dy^{III} ions (Dy^{III}–N≡C–Co^{III}). Each Co^{III} has six bonds to carbon atoms of the μ_2-CN^- groups. The neighboring Dy^{III} ions of the Dy1···Dy2 and Dy3···Dy4 are triply bridged by the oxygen atoms of three μ_2-(benpyo) ligands. Atoms O5, O7, and O9 bridge Dy1 and Dy2, and atoms O17, O25, and O27 bridge Dy3 and Dy4 (see Table S2). The 4-benpyo ligands comprising atoms O1, O3, O11, O13, O15, O19, O21, O23, O29, O31, and O33 are bound terminally to a Dy^{III} center. Thus, 11 4-benpyo ligands are terminal, each forming a coordination bond with one 4f-metal ion, whereas six 4-benpyo ligands each bridges two neighboring Dy^{III} centers. A terminal aquo ligand (O35) completes eight coordination at Dy1. The coordination spheres are of the $\{Co^{III}C_6\}$ and $\{Dy^{III}N_2O_6\}$ types. The Co^{III}–C [1.879(6)–1.927(8) Å] bond lengths correspond to low-spin, six-coordinate Co^{III} ions while the Dy^{III}–N cyanido [2.440(5)–2.462(4) Å] bond lengths are indicative of eight-coordinate Dy^{III} ions, linked by cyanido groups. The Dy^{III}–O bond lengths [2.261(4)–2.518(4) Å] are also typical of eight-coordinate Dy^{III} centers.[16,36] The Co–C≡N groups are almost linear, the corresponding angles being in the 175.8(10)–179.8(7)° range. The Dy–NC≡NC angles are in the 165.6(5)–172.0(4)° range suggesting a bending of this group. The Dy–O terminal bonds [average: 2.291(4) Å] are shorter than the Dy–O bridging bonds [average: 2.432(4) Å], as expected.

The coordination geometries of the Co^{III} centers are almost perfect octahedral. The trans C–Co^{III}–C angles for Co1, Co2, and Co3 are in the ranges 178.1(3)–179.1(3),178.1(3)–179.0(3), and 178.6(3)–179.3(3)°, respectively; those for Co4 and Co5 are exactly 180.0° because these metal ions sit on symmetry centers. The coordination polyhedra of the eight-coordinate Dy^{III} ions were evaluated by applying the program SHAPE.[48] The $Dy^{III}N_2O_6$ coordination polyhedra around Dy1, Dy3, and Dy4 are described as dodecahedra with least continuous shape measures (CShM) values of 1.256, 1.230, and 0.899, respectively. The polyhedron for Dy2 appears to be intermediate between the dodecahedron (CShM value of 1.341) and the biaugmented trigonal prism (CShM value of 1.445). Numerical values are listed in Table S3. The same conclusions are also reached by applying the angular criteria established by Kepert.[49]

The crystal structure of the compound is stabilized by strong hydrogen bonds involving the monodentate cyanides of the hexacyanocobaltate groups and the H_2O molecules. In addition, several weak C–H···O/N interactions complement the rigidity of the structure (Table S4).

Overall, the crystal structure of the compound can be described as a uninodal net consisting of four-coordinated nodes. Specifically, each $[Dy_2]$ unit can be described as a four-coordinated node which is connected through the linear linkers $[Co(CN)_6]^{3-}$ to four neighboring units (Figure S3). Thus, the topology of the compound is dictated by the connectivity of the Dy_2 unit (Figure S4). The geometry of the $[Dy_2]$ units is tetrahedral, thus leading to the formation of a **dia** net (Figure S5).

Magnetic Measurements. The magnetic properties of compound **1** were investigated through magnetic susceptibility measurements employing a SQUID magnetometer. The room-temperature static magnetic susceptibility $\chi_M T(T)$ value for the powdered sample in an applied field of 1 kOe revealed a value of 56.76 $cm^3\ mol^{-1}\ K$ in accordance with the value of 56.68 $cm^3\ mol^{-1}\ K$ which is expected for four uncoupled Dy^{III} ions ($^6H_{15/2}$, $J = 15/2$, $g = 4/3$) (Figure 2A). The $\chi_M T(T)$ profile

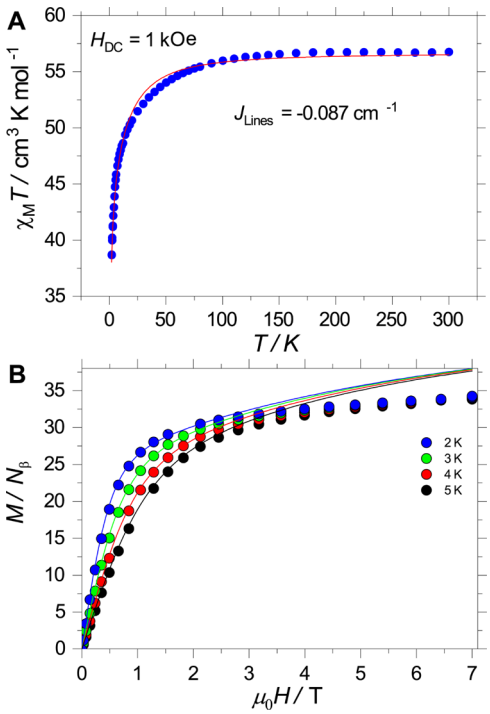

Figure 2. (A) Experimental $\chi_M T(T)$ and (B) $M(H)$ for compound **1**, collected employing a powdered sample and with H_{DC} = 1 kOe. Solid lines are fit to the Lines model (see text for details).

remains practically constant down to ca. 100 K where it starts decreasing reaching a $\chi_M T(T)$ value of 38.67 $cm^3\ mol^{-1}\ K$ at 2 K. The decrease in $\chi_M T(T)$ can be ascribed to depopulation of the crystal field levels and antiferromagnetic interactions between the nearest Dy···Dy centers (*vide infra*). $M(H)$ measurements between 0 and 7 T and 2 and 5 K show significant anisotropy and a lack of saturation with the largest $M(H)$ value at 2 K being 34.36 μ_B (8.6 μ_B per Dy^{III} ion) (Figure 2B), which is larger than the expected value for the ideal Dy^{III} with pure m_J = 15/2, i.e., 5.8 μ_B per Dy^{III} ion, indicating strong anisotropy.

The slow relaxation dynamics of **1** were likewise studied in a SQUID magnetometer employing alternating current (AC) magnetic susceptibility measurements (Figures 3, S6, and S7). At zero DC field, no SMM behavior was observed. In contrast, the application of an optimal field of 2 kOe reveals the SMM character in **1** with a clear frequency-dependent out-of-phase maximum between 2 and 7.2 K as shown for $\chi_M''(T)$ (Figures

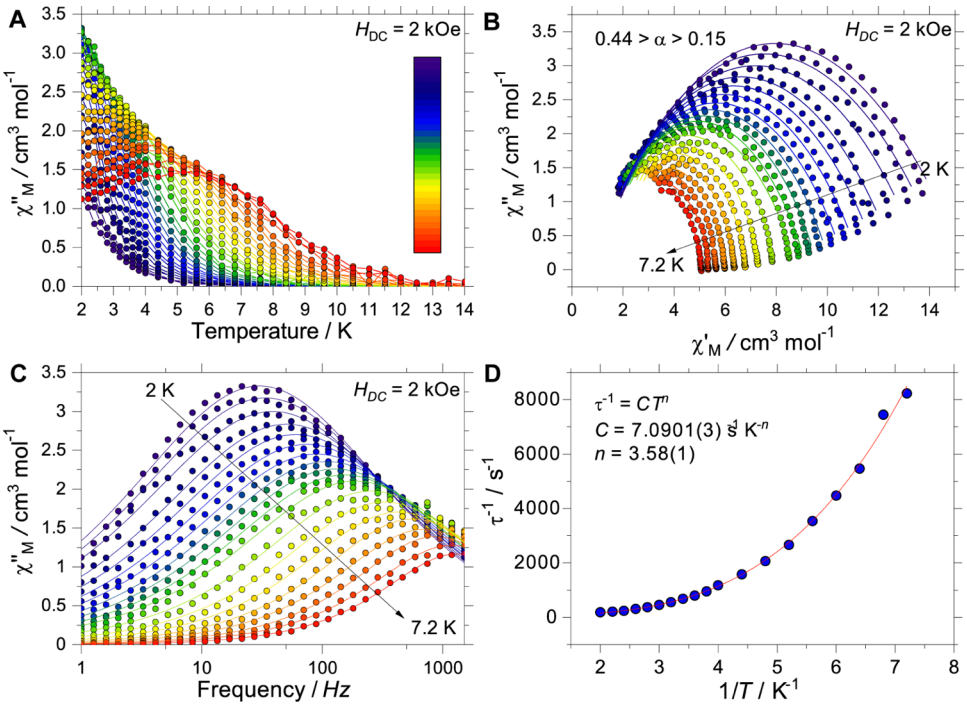

Figure 3. Dynamic magnetic susceptibility data for **1**: (A) experimental $\chi_M''(T)$, (B) Cole−Cole plots, (C) $\chi_M''(\nu)$ with an applied optimal field H_{DC} = 2 kOe and an oscillating field of 3.5 Oe for temperatures between 2 and 7.2 K, and (D) extracted $\tau(T)$ data and fit considering solely the Raman process.

3A and S8). The maximum in $\chi_M''(\nu)$ shifts toward higher frequencies upon increasing temperatures (Figure 3C), marking the temperature-dependent regime. Fitting the $\chi_M''(\nu)$ and $\chi_M'(\nu)$ to a single process simultaneously (Figure 3B,C and Table S5) allows extraction of $\tau(T)$ and α oscillating between 0.44 and 0.15, revealing a wide distribution of processes. As observed in Figure 3D, the $\tau(T)$ can be reproduced solely considering the Raman process $\tau^{-1} = CT^n$ with the following parameters: C = 7.0901(3) s^{-1} K^{-n}, n = 3.58(1), as often observed for light lanthanide SMMs.[50−52] Note that n is smaller than expected for Kramers ions, i.e., n = 9, indicating that a high density of low-lying states as well as optical and acoustic phonons play a major role in the relaxation mechanism.[53,54] This is consistent with the lack of SMM characteristics at zero field, indicative of fast relaxation.

The slow relaxation character of **1** was further confirmed by μ-SQUID measurements which were performed in the temperature range of 1.5 K−30 mK and between ±1 T while the rates of the field sweep were in the range of 1−64 mT/s (Figure 4A,B). Single crystals of compound **1** were carefully selected for the magnetic measurements while the external magnetic field was aligned parallel to the easy axis of the crystals (transverse field method).[55,56] The curves show a very narrow loop, highlighting very fast relaxation. The strong quantum tunneling of the magnetization (QTM) is confirmed by the following experimental evidence: (a) temperature dependence of the magnetization loops, (b) sweep-field dependence of the loops, (c) small opening of the loops at 30 mK, (d) very fast scan rates, and (e) sharp transition at zero magnetic field. The results of the μ-SQUID studies are in accordance with the AC measurements, where the SMM behavior of compound **1** was observed only upon application of a non-zero DC field. A closer inspection of the loops reveals a small S-shaped near-zero field (Figure 4B,D), commonly observed for coupled dimers.[57] The S-shaped loops allow for the extraction of the mean exchange field (H_{ex}) from the inflexion points in the hysteresis loops with $H_{ex} = -2J_{ex}m_J/g_J\mu_B$, where g_J = 4/3 and m_J = 15/2. The determined interaction obtained is found to be J_{ex} = −1.4 mK. The experimentally obtained value is smaller than expected from a purely dipolar interaction analysis for two Ising Dy^{III} ions with m_J = 15/2 at a distance of 3.8571(6) Å, i.e., 9 mK. The different dipolar interaction values, compared to the one obtained from the mean field analysis, and the $M(H)$ profile indicate that the ground state of Dy^{III} is not necessarily pure m_J = 15/2 for both ions and that there might be an interaction operating between the Dy^{III} ions.

Ab Initio Calculations. To comprehend the magnetic characteristics of compound **1**, *ab initio* calculations were carried out using the OpenMolcas package[58−61] and employing the CASSCF/SO-RASSI/SINGLE_ANISO approach. Due to the large size of **1**, and considering the structure of the compound, a Dy_2 fragment of the molecule was employed for the calculations (Figure 5). The crystal structure was employed for the calculations without further optimizations, and the standard basis sets from the ANO-RCC library[59−61] were used for the description of the atoms. The basis set of VTZP quality was employed for the Dy^{III} ions, while for the atoms directly bound to the Dy^{III} ions and for all of the remaining atoms, the VDZP and VDZ quality was used, respectively. Optimization of the molecular orbitals was carried out by state-averaged CASSCF calculations. Three calculations were carried out (RASSCF routine) with 21, 224, and 490 states for S = 5/2, S = 3/2, and S = 1/2, respectively. The CASSCF wavefunctions were subsequently mixed by spin−orbit coupling, employing the RASSI routine with all 21 states for S = 5/2 being included, while 128 and 130 states were included for S = 3/2 and S = 1/2, respectively. Finally, the SINGLE_ANISO module[59] was

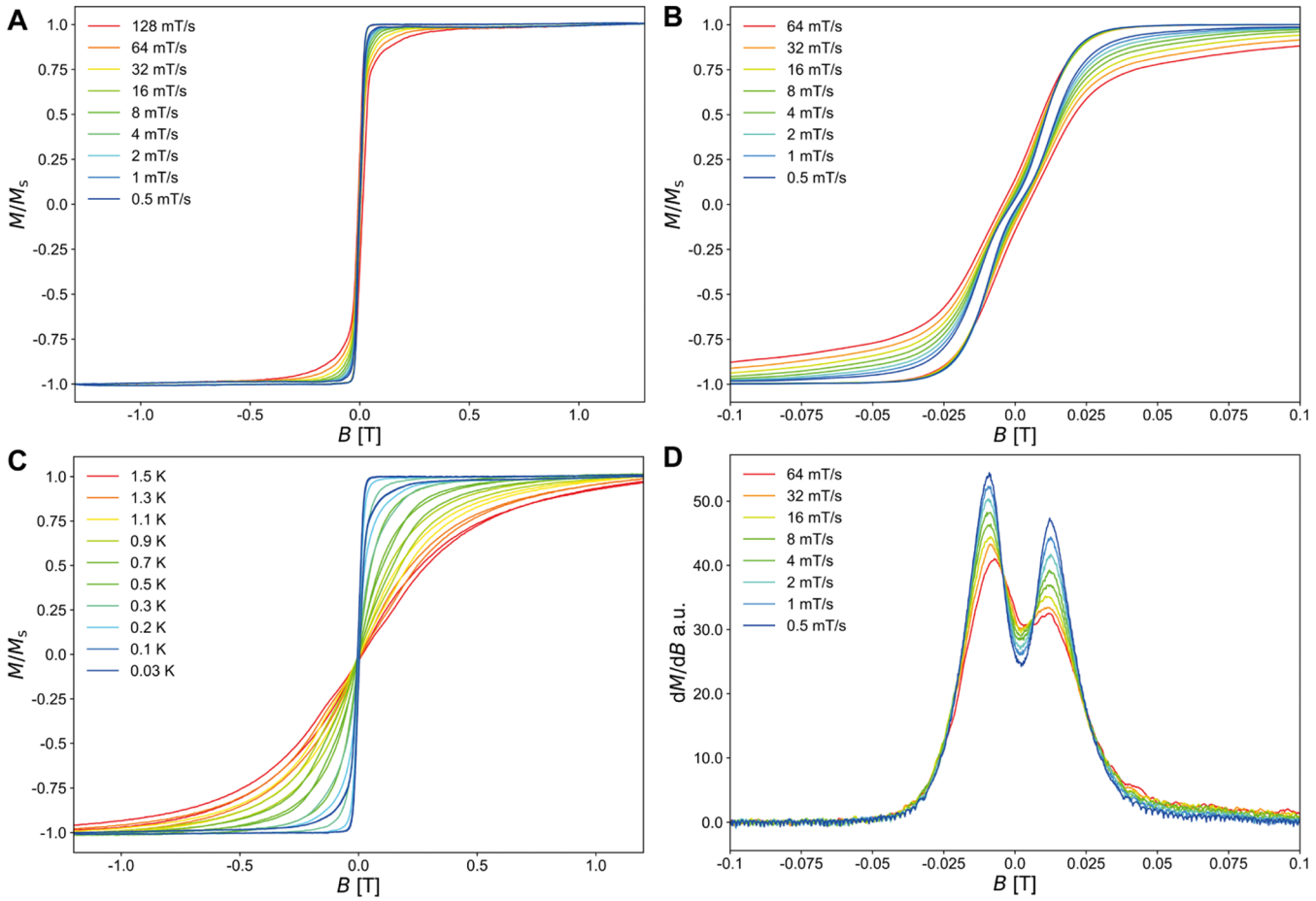

Figure 4. μ-SQUID loops collected on a single crystal of **1** with the applied field along the easy axis of the crystal. (A) Loops collected at 30 mK and at different field-sweep rates. (B) Magnification of the loops collected at 30 mK. (C) Temperature dependent of the loops at a fixed sweeping rate of 64 mT/s. (D) Derivative of the loops shown in panel (B).

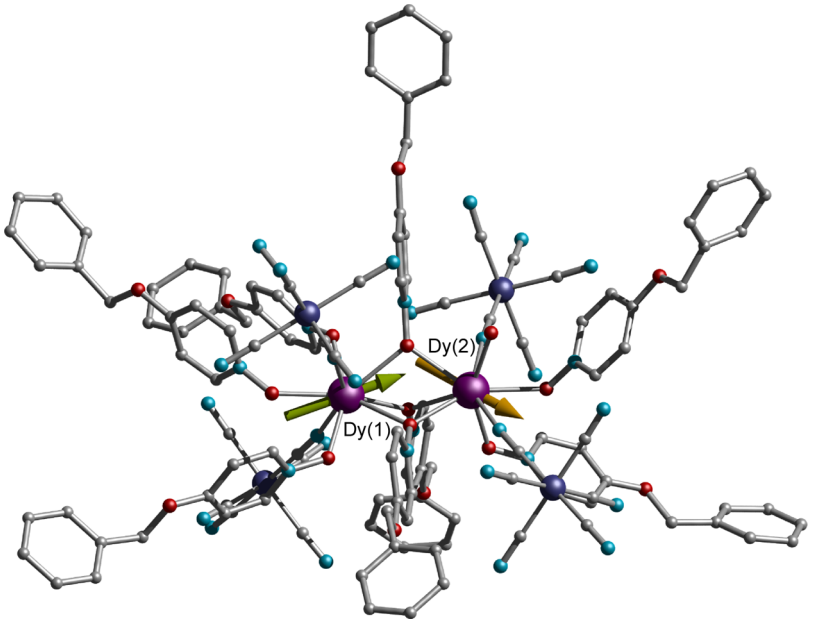

Figure 5. Directions of the main axes of the *g*-tensors in the ground Kramer doublet of compound **1** for Dy(1) (green arrow) and Dy(2) (orange arrow). Color code: Co, cyan; Dy, purple; O, red; C, black; and N, pale blue. Hydrogens are omitted for clarity.

employed for the calculation of the crystal field decomposition of the ground $J = 15/2$ multiplet of the $^6H_{15/2}$ term.

Two distinct Dy^{III} ions can be identified in the compound (see Figure 5), possessing distinct electronic characteristics, as

shown by CASSCF. It was found that the g values of the ground doublet state of Dy(1) are g_x = 0.2223, g_y = 0.3222, and g_z = 19.1582, indicating an Ising behavior with m_J = 15/2 (Table S6). The energy difference of the first, second, and third excited states is 46, 74, and 83 cm^{-1}, respectively. In Figure 5 is shown also the main magnetic axis (z) on the Dy(1) with a green arrow. In contrast, very distinct characteristics are found for Dy(2), with the g values being g_x = 0.5242, g_y = 1.9617, and g_z = 17.4850; the g values are indicative of a mixed state (Tables S6 and S7). For comparison reasons, the main magnetic axis (z) on the Dy(2) ion is also presented in the same figure using an orange arrow.

Note that there is a spin canting of ca. 58° between Dy(1) and Dy(2). This type of canting, along with magnetic interactions is known to induce fast relaxation in SMMs.[62] The energy difference of the first, second, and third excited states of Dy(2) is 34, 72, and 133 cm^{-1}, respectively. Wavefunction analysis shows that for Dy(1) the ground doublet possesses a large m_J = 15/2 component, while for Dy(2) the m_J composition is highly mixed. The observed fast relaxing characteristics of **1** are in accordance with the average configuration of the matrix elements of magnetic moment between the electronic states, revealing that in the ground state and through excites states relaxation is possible. The profile of the magnetic loops is typical for antiferromagnetically coupled Ising-like spins.[57,63,64]

With the knowledge of the crystal field parameters, derived from the theoretical CASSCF calculation, it is possible to quantify the interaction operating between the Dy^{III} ion. Fitting of the magnetic susceptibility[65] was performed, employing the Lines model[66] with the form

$$\hat{H} = \sum_{k=2,4,6}\sum_{q=-k}^{k}(B^{q}_{kDy(1)}\hat{O}^{q}_{kDy(1)} + B^{q}_{kDy(2)}\hat{O}^{q}_{kDy(2)}) - 2J_{Lines}(S_{Dy(1)}\cdot S_{Dy(2)}) + \mu_B g_J(\hat{J}_{Dy(1)}\cdot I + \hat{J}_{Dy(2)}\cdot I)\cdot \mu_0 H \quad (2)$$

where the first term represents the crystal field parameters, $B^{q}_{kDy(1)}$, and the operators, $\hat{O}^{q}_{kDy(1)}$. The second term represents the Lines interaction connecting the isotropic component (S = 5/2) of the angular momenta for Dy^{III} and the last term is the Zeeman term. By fitting the $\chi_M T(T)$ experimental data, good agreement is found for J_{Lines} = −0.087 cm^{-1} (−0.125 K) for $\chi_M T(T)$ and $M(H)$ (Figure 2A,B) ($R = \sum_i^N [(\chi_M T)_{obs} - (\chi_M T)_{calc}]^2$ = 0.20%). The experimental exchange value derived from μ-SQUID loops is not comparable to the value obtained from the theoretical Lines analysis. Note that although $\chi_M T(T)$ is well reproduced by the Lines model and the crystal field parameters obtained from CASSCF calculations, the $M(H)$ simulated traces are not superimposable with the experimental data. This highlights the anisotropic nature of **1** and the limitations of CASSCF calculations, in which intermolecular interactions and packing effects are not considered.[67]

With the full picture at hand, i.e., magnetic data and CASSCF calculations, it is possible to understand the dynamic magnetic properties of **1**. Magnetic AC susceptibility measurements at zero field show no SMM behavior indicating fast relaxation operating in **1**, while μ-SQUID loops show a very narrow opening, both consistent with CASSCF calculations: (i) a small separation is observed for both Dy(III) ions in **1**; (ii) while Dy(1) shows a pure m_J = 15/2, the wavefunction for Dy(2) is highly mixed; and (iii) the non-negligible transition matrix elements and the spin canting between Dy(1) and Dy(2) (58°), all contribute to a very fast relaxation in **1**. The application of an optimal field of 2 kOe reduces relaxation, acting also as decoupling field, revealing the relaxation characteristic arising from **1**. Note that due to the low-lying excited states which induce fast relaxation, the $\tau(T)$ can be solely reproduced employing the Raman process.

Luminescence Study. Compounds **1** and **2** display luminescence at temperatures between 14 and 300 K, as shown in Figures 6 and S9, respectively. The emission spectra

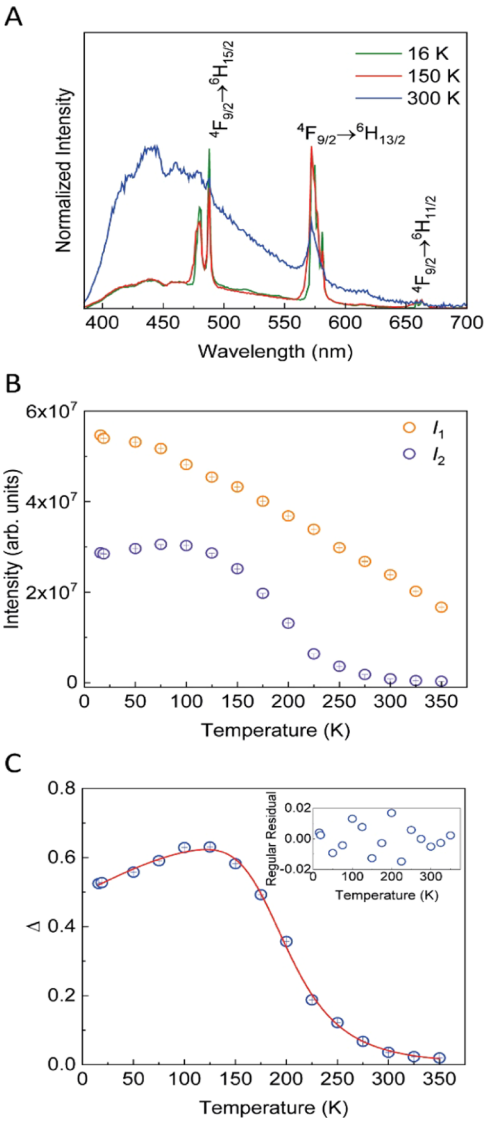

Figure 6. (A) Emission spectra (excitation at 365 nm) of compound **1** at selected temperatures. (B) I_1 and I_2 as function of the temperature. (C) Temperature dependence of the thermometric parameter; the red line represents the best fit to eq 4. In the inset is shown the fit regular plot.

of compound **2** show the characteristic $^5D_0 \rightarrow {}^7F_{1-4}$ transitions of Eu^{III} ions, as illustrated in Figure S9A. The corresponding excitation spectra, monitored within the more intense $^5D_0 \rightarrow {}^7F_2$ transition, display the intra-$4f^6$ lines overlapped with a broadband (250−400 nm) ascribed to the ligand excitation (Figure S9B). The compound can be used as a luminescence

thermometer based on the temperature dependence of their excitation spectra (as the emission ones show a very weak temperature dependence). Examples of ratiometric luminescent thermometers based on the excitation spectra of Ln^{III} ions are scarce[68−71] as these thermometers require more elaborated equipment and longer acquisition times, being this a disadvantage relatively to those based on the emission spectra.[72] We consider the ratio between the 240−450 nm (I_A) and 450−480 nm (I_B) integrated intensity areas of the excitation spectra (Figure S9B). The defined thermometric parameter is well described by a polynomial function, eq S5, allowing compound **2** to operate as a thermometer in the 25−325 K range with a temperature uncertainty (δT)[73] lower than 1 K in the 75−325 K range and S_r = 0.6%·K^{-1} at around 325 K (Table S8 and Figures S10 and S11). This value is lower than those reported for other Eu^{III}-based thermometers based on the excitation spectra.[68−71]

A higher S_r value is obtained using the temperature dependence of the emission spectra of compound **1**. The low-temperature emission spectra of compound **1** reveal the characteristic $^4F_{9/2} \rightarrow {}^6H_{15/2-11/2}$ transitions of Dy^{III} ions together with a broadband between 400 and 600 nm related to the emission of the ligands (Figure 6A). Self-absorption transitions are observed in the emission spectrum at 425 ($^4H_{11/2} \rightarrow {}^4G_{11/2}$), 450 ($^4H_{11/2} \rightarrow {}^4H_{15/2}$), and 471 nm ($^4H_{11/2} \rightarrow {}^4F_{9/2}$) that result from the so-called "inner filter effect," indicating radiative energy transfer from the ligands to the Dy^{III} ions.[74] This effect is observed in luminescence whenever one of the components of the system has absorptions which overlap the luminescence of the other(s). This results in a diminution of the luminescence at those wavelengths and this has been already observed both in solution and in solid state.[74,75] As the temperature increases the relative intensity of the Dy^{III} lines decreases. The excitation spectra monitored within the more intense $^4F_{9/2} \rightarrow {}^6H_{13/2}$ transition reveal the intra-$4f^9$ lines of Dy^{III} ions, as illustrated in Figure S12.

Taking advantage of the dependence of the emission spectra on the temperature and aiming to explore the thermometric features of compound **1**, we define a thermometric parameter

$$\Delta = \frac{I_1}{I_2} \tag{3}$$

where I_1 and I_2 correspond to the ligand and Dy^{III} emission intensities, respectively.

While I_2 was determined by integrating the emission spectra between 470 and 500 nm, 550 and 590 nm, and 650 and 675 nm after performing a baseline correction to remove the ligands' emission, I_1 was calculated by subtracting to the integrated intensity of the emission spectra between 385 and 700 nm the I_2 contribution. No correction was performed to account for the small contribution of the self-absorption transitions observed in the ligand band at higher temperatures. The classical Mott−Seitz model involving one deactivation channel[14] can be used to describe the Dy^{III} emission (I_2), while I_1 is well described by a second-degree polynomial function (Figure 6B). Therefore, $\Delta(T)$ is well described in the 16−350 K range by

$$\Delta = \frac{\frac{\Delta_0}{1 + \alpha e^{-\Delta E/k_B T}}}{A + BT + CT^2} \tag{4}$$

where k_B is the Boltzmann constant, T is the absolute temperature, and ΔE is the activation energy for the thermal quenching process. The fitting results are shown as a solid line in the temperature dependence of Δ (Figure 6C) while the values obtained from the fitting of eq 4 are presented in Table S9. The relative thermal sensitivity presents an S_r = 2.3%·K^{-1} at around 240 K and δT = 0.1 K (Figure S13). When compared with the few other polycyanidometallate-based SMM luminescent thermometers in which the thermometric operation was studied, compound **1** presents a broader operation range with a higher S_r than the 0-D $[DyCo^{III}(CN)_6(bpyO_2)_2(H_2O)_3]\cdot 4H_2O$, 1.84% K^{-1} at 70 K,[33] and an S_r similar to that of the 2-D $\{[Tb_{0.5}Dy_{0.5}(4\text{-}OHpy)_2(H_2O)_3]\ [Co^{III}(CN)_6]\}$, S_r = 2.2(3) % K^{-1} at 170 K.[15]

CONCLUSIONS

We reported here for the first time, two new 3-D polycyanidometallate-based luminescent thermometers with the formula $\{Ln_4Co_4(CN)_{24}(4\text{-benpyo})_{17}(H_2O)\cdot 7H_2O\}_n$ Ln = (Dy^{III}(**1**), Eu^{III}(**2**)). Magnetic AC measurements indicate that at zero field no SMM behavior is observed due to fast relaxation operating in **1**, while μ-SQUID loops show a very narrow opening in accordance with the following CASSCF results: (a) small energy separations of states for both distinct Dy(III) ions, Dy(1) and Dy(2), of compound **1**; (b) a pure m_J = 15/2 wavefunction for Dy(1) vs a highly mixed for Dy(2) ion; and (c) the non-negligible transition matrix elements and the spin canting between Dy(1) and Dy(2) (58°). The SMM character of compound **1** is introduced upon application of an optimal field of 2 kOe while the τ(T) is reproduced considering the Raman process indicating that the major role in the relaxation mechanism of compound **1** is due to the high density of low-lying states and optical and acoustic phonons. The interaction between the Dy^{III} ions is found to be J_{Lines} = −0.087 cm^{-1} (−0.125 K) by fitting the experimental χ_MT(T) and $M(H)$, using the Lines model and the CASSCF-calculated crystal field parameters. Compound **2** is a luminescent thermometer based on the excitation spectra operating in the 25−325 K range with a maximum S_r = 0.6% K^{-1} at 325 K. Compound **1**, on the other hand, displays temperature-dependent emission features that were used to define a luminescent thermometer operating in the temperature range of 16−350 K with S_r = 2.3% K^{-1} at 240 K. This work highlights new synthetic pathways toward a new generation of cleverly designed 3-D SMM luminescent thermometers.

ASSOCIATED CONTENT

Accession Codes

CCDC 2194059 contains the supplementary crystallographic data for this paper. These data can be obtained free of charge via www.ccdc.cam.ac.uk/data_request/cif, or by emailing data_request@ccdc.cam.ac.uk, or by contacting The Cambridge Crystallographic Data Centre, 12 Union Road, Cambridge CB2 1EZ, UK; fax: +44 1223 336033.

AUTHOR INFORMATION

Corresponding Authors

Vassilis Tangoulis − *Department of Chemistry, Laboratory of Inorganic Chemistry, University of Patras, 26504 Patras,*

Greece; orcid.org/0000-0002-2039-2182; Email: vtango@upatras.gr

Eufemio Moreno-Pineda – *Departamento de Química-Física, Facultad de Ciencias Naturales, Exactas y Tecnología, Universidad de Panamá, Panama City 0824, Panama*; orcid.org/0000-0002-9643-0341; Email: eufemio.moreno@up.ac.pa

Wolfgang Wernsdorfer – *Institute for Quantum Materials and Technology (IQMT), Karlsruhe Institute of Technology (KIT), D-76344 Eggenstein-Leopoldshafen, Germany; Physikalisches Institut, Karlsruhe Institute of Technology, D-76131 Karlsruhe, Germany*; orcid.org/0000-0003-4602-5257; Email: wolfgang.wernsdorfer@kit.edu

Luis D. Carlos – *Phantom-g, CICECO – Aveiro Institute of Materials, Department of Physics, University of Aveiro, 3810-193 Aveiro, Portugal*; orcid.org/0000-0003-4747-6535; Email: lcarlos@ua.pt

Authors

Konstantinos Karachousos-Spiliotakopoulos – *Department of Chemistry, Laboratory of Inorganic Chemistry, University of Patras, 26504 Patras, Greece*; orcid.org/0000-0003-2030-4733

Nikos Panagiotou – *Department of Chemistry, University of Cyprus, Nicosia 1678, Cyprus*; orcid.org/0000-0003-1786-326X

Anastasios Tasiopoulos – *Department of Chemistry, University of Cyprus, Nicosia 1678, Cyprus*; orcid.org/0000-0002-4804-3822

Vassilis Nastopoulos – *Department of Chemistry, Laboratory of Inorganic Chemistry, University of Patras, 26504 Patras, Greece*

Michael Schulze – *Physikalisches Institut, Karlsruhe Institute of Technology, D-76131 Karlsruhe, Germany*; orcid.org/0000-0002-7169-0630

Alexandre M. P. Botas – *Phantom-g, CICECO – Aveiro Institute of Materials, Department of Physics, University of Aveiro, 3810-193 Aveiro, Portugal; i3N-Institute for Nanostructures, Nanomodelling and Nanofabrication, Department of Physics, University of Aveiro, 3810-193 Aveiro, Portugal*

Notes

The authors declare no competing financial interest.

ACKNOWLEDGMENTS

This work was developed within the scope of the project CICECO-Aveiro Institute of Materials, UIDB/50011/2020, UIDP/50011/2020, and LA/P/0006/2020, financed by national funds through the FCT/MEC (PIDDAC). E.M.-P. thanks the Panamanian National System of Investigators (SNI) and SENACYT (Project PFID-FID-2021-60) for support. W.W. thanks the Alexander von Humboldt Foundation and the ERC Advanced Grant MoQuOS.

REFERENCES

(1) Allison, S. W. A Brief History of Phosphor Thermometry. *Meas. Sci. Technol.* **2019**, *30*, No. 072001.

(2) Brites, C. D. S.; Lima, P. P.; Silva, N. J. O.; Millán, A.; Amaral, V. S.; Palacio, F.; Carlos, L. D. Thermometry at the Nanoscale. *Nanoscale* **2012**, *4*, 4799.

(3) Sun, H.; Wu, X.; Peng, D.; Kwok, K. Room-Temperature Large and Reversible Modulation of Photoluminescence by in Situ Electric Field in Ergodic Relax or Ferroelectrics. *ACS Appl. Mater. Interfaces* **2017**, *9*, 34042−34049.

(4) Coronado, E.; Galán-Mascarós, J. R.; Gómez-García, C. J.; Laukhin, V. Coexistence of Ferromagnetism and Metallic Conductivity in a Molecule-Based Layered Compound. *Nature* **2000**, *408*, 447−449.

(5) Long, J.; Rouquette, J.; Thibaud, J.-M.; Ferreira, R. A. S.; Carlos, L. D.; Donnadieu, B.; Vieru, V.; Chibotaru, L. F.; Konczewicz, L.; Haines, J.; Guari, Y.; Larionova, J. A High-Temperature Molecular Ferroelectric Zn/Dy Complex Exhibiting Single-Ion-Magnet Behavior and Lanthanide Luminescence. *Angew. Chem.* **2015**, *127*, 2264−2268.

(6) Darawsheh, M.; Barrios, L. A.; Roubeau, O.; Teat, S. J.; Aromí, G. Encapsulation of a Cr III Single-Ion Magnet within an Fe II Spin-Crossover Supramolecular Host. *Angew. Chem., Int. Ed.* **2018**, *57*, 13509−13513.

(7) Ferreira, R. A. S.; Mamontova, E.; Botas, A. M. P.; Shestakov, M.; Vanacken, J.; Moshchalkov, V.; Guari, Y.; Chibotaru, L. F.; Luneau, D.; André, P. S.; Larionova, J.; Long, J.; Carlos, L. D. Synchronous Temperature and Magnetic Field Dual-Sensing by Luminescence in a Dysprosium Single-Molecule Magnet. *Adv. Opt. Mater.* **2021**, *9*, No. 2101495.

(8) Goodwin, C. A. P.; Ortu, F.; Reta, D.; Chilton, N. F.; Mills, D. P. Molecular Magnetic Hysteresis at 60 Kelvin in Dysprosocenium. *Nature* **2017**, *548*, 439−442.

(9) Guo, F.-S.; Day, B. M.; Chen, Y.-C.; Tong, M.-L.; Mansikkamäki, A.; Layfield, R. A. Magnetic Hysteresis up to 80 Kelvin in a Dysprosium Metallocene Single-Molecule Magnet. *Science* **2018**, *362*, 1400−1403.

(10) Gaita-Ariño, A.; Luis, F.; Hill, S.; Coronado, E. Molecular Spins for Quantum Computation. *Nat. Chem.* **2019**, *11*, 301−309.

(11) Bünzli, J.-C.; Piguet, C. Taking Advantage of Luminescent Lanthanide Ions. *Chem. Soc. Rev.* **2005**, *34*, 1048.

(12) Carlos, L. D.; Ferreira, R. A. S.; Bermudez, V.; Ribeiro, S. J. L. Lanthanide-Containing Light-Emitting Organic-Inorganic Hybrids: A Bet on the Future. *Adv. Mater.* **2009**, *21*, 509−534.

(13) Eliseeva, S. V.; Bünzli, J.-C. G. Lanthanide Luminescence for Functional Materials and Bio-Sciences. *Chem. Soc. Rev.* **2010**, *39*, 189−227.

(14) Rocha, J.; Brites, C. D. S.; Carlos, L. D. Lanthanide Organic Framework Luminescent Thermometers. *Chem. – Eur. J.* **2016**, *22*, 14782−14795.

(15) Kumar, K.; Chorazy, S.; Nakabayashi, K.; Sato, H.; Sieklucka, B.; Ohkoshi, S. I. TbCo and $Tb_{0.5}Dy_{0.5}Co$ Layered Cyanido-Bridged Frameworks for Construction of Colorimetric and Ratiometric Luminescent Thermometers. *J. Mater. Chem. C* **2018**, *6*, 8372−8384.

(16) Long, J.; Guari, Y.; Ferreira, R. A. S.; Carlos, L. D.; Larionova, J. Recent Advances in Luminescent Lanthanide Based Single-Molecule Magnets. *Coord. Chem. Rev.* **2018**, *363*, 57−70.

(17) Chorazy, S.; Rams, M.; Nakabayashi, K.; Sieklucka, B.; Ohkoshi, S. I. White Light Emissive DyIII Single-Molecule Magnets Sensitized by Diamagnetic $[Co^{III}(CN)_6]^{3-}$ Linkers. *Chem. – Eur. J.* **2016**, *22*, 7371−7375.

(18) Wang, J.; Chorazy, S.; Nakabayashi, K.; Sieklucka, B.; Ohkoshi, S. I. Achieving White Light Emission and Increased Magnetic Anisotropy by Transition Metal Substitution in Functional Materials Based on Dinuclear Dy^{III}(4-Pyridone)$[M^{III}(CN)_6]^{3-}$ (M = Co, Rh) Molecules. *J. Mater. Chem. C* **2018**, *6*, 473−481.

(19) Chorazy, S.; Kumar, K.; Nakabayashi, K.; Sieklucka, B.; Ohkoshi, S. I. Fine Tuning of Multicolored Photoluminescence in Crystalline Magnetic Materials Constructed of Trimetallic $Eu_xTb_{1-x}[Co(CN)_6]$ Cyanido-Bridged Chains. *Inorg. Chem.* **2017**, *56*, 5239−5252.

(20) Pointillart, F.; Guennic, B.; Golhen, S.; Cador, O.; Maury, O.; Ouahab, L. A Redox-Active Luminescent Ytterbium Based Single Molecule Magnet. *Chem. Commun.* **2013**, *49*, 615−617.

(21) Chorazy, S.; Rams, M.; Wang, J.; Sieklucka, B.; Ohkoshi, S. I. Octahedral Yb(III) Complexes Embedded in $[Co^{III}(CN)_6]$-bridged

coordination chains: combining sensitized near-infrared fluorescence with slow magnetic relaxation. *Dalton Trans.* **2017**, *46*, 13668−13672.
(22) Jankowski, R.; Zakrzewski, J. J.; Surma, O.; Ohkoshi, S. I.; Chorazy, S.; Sieklucka, B.; Near-Infrared. Emissive Er(III) and Yb(III) Molecular Nanomagnets in Metal-Organic Chains Functionalized by Octacyanidometallates(IV). *Inorg. Chem. Front.* **2019**, *6*, 2423−2434.
(23) Pointillart, F.; Le Guennic, B.; Cador, O.; Maury, O.; Ouahab, L. Lanthanide Ion and Tetrathiafulvalene-Based Ligand as a "Magic" Couple toward Luminescence, Single Molecule Magnets, and Magnetostructural Correlations. *Acc. Chem. Res.* **2015**, *48*, 2834−2842.
(24) Li, Q.-W.; Liu, J.-L.; Jia, J.-H.; Chen, Y.-C.; Liu, J.; Wang, L.-F.; Tong, M.-L. "Half-Sandwich" Yb III Single-Ion Magnets with Metallacrowns. *Chem. Commun.* **2015**, *51*, 10291−10294.
(25) Soussi, K.; Jung, J.; Pointillart, F.; Le Guennic, B.; Lefeuvre, B.; Golhen, S.; Cador, O.; Guyot, Y.; Maury, O.; Ouahab, L. Magnetic and Photo-Physical Investigations into Dy^{III} and Yb^{III} Complexes Involving Tetrathiafulvalene Ligand. *Inorg. Chem. Front.* **2015**, *2*, 1105−1117.
(26) Jia, J.-H.; Li, Q.-W.; Chen, Y.-C.; Liu, J.-L.; Tong, M.-L. Luminescent Single-Molecule Magnets Based on Lanthanides: Design Strategies, Recent Advances and Magneto-Luminescent Studies. *Coord. Chem. Rev.* **2019**, *378*, 365−381.
(27) Brunet, G.; Marin, R.; Monk, M.-J.; Resch-Genger, U.; Gálico, D. A.; Sigoli, F. A.; Suturina, E. A.; Hemmer, E.; Murugesu, M. Exploring the Dual Functionality of an Ytterbium Complex for Luminescence Thermometry and Slow Magnetic Relaxation. *Chem. Sci.* **2019**, *10*, 6799−6808.
(28) Errulat, D.; Marin, R.; Gálico, D. A.; Harriman, K. L. M.; Pialat, A.; Gabidullin, B.; Iikawa, F.; Couto, O. D. D.; Moilanen, J. O.; Hemmer, E.; Sigoli, F. A.; Murugesu, M. A Luminescent Thermometer Exhibiting Slow Relaxation of the Magnetization: Toward Self-Monitored Building Blocks for Next-Generation Optomagnetic Devices. *ACS Cent. Sci.* **2019**, *5*, 1187−1198.
(29) Kumar, K.; Abe, D.; Komori-Orisaku, K.; Stefańczyk, O.; Nakabayashi, K.; Shakirova, J. R.; Tunik, S. P.; Ohkoshi, S. Neodymium β-Diketonate Showing Slow Magnetic Relaxation and Acting as a Ratiometric Thermometer Based on near-Infrared Emission. *RSC Adv.* **2019**, *9*, 23444−23449.
(30) Fondo, M.; Corredoira-Vazquez, J.; Garcia-Deibe, A. M.; Sanmartin-Matalobos, J.; Amoza, M.; Botas, A. M. P.; Ferreira, R. A. S.; Carlos, L. D.; Colacio, E. Field-Induced Slow Magnetic Relaxation and Luminescence Thermometry in a Mononuclear Ytterbium Complex. *Inorg. Chem. Front.* **2020**, *7*, 3019−3029.
(31) Zakrzewski, J. J.; Liberka, M.; Zychowicz, M.; Chorazy, S. Diverse Physical Functionalities of Rare-Earth Hexacyanidometallate Frameworks and Their Molecular Analogues. *Inorg. Chem. Front.* **2021**, *8*, 452−483.
(32) Zhang, Y.; Guo, Z.; Xie, S.; Li, H. L.; Zhu, W. H.; Liu, L.; Dong, X. Q.; He, W. X.; Ren, J. C.; Liu, L. Z.; Powell, A. K. Tuning the Origin of Magnetic Relaxation by Substituting the 3d or Rare-Earth Ions into Three Isostructural Cyano-Bridged 3d-4f Heterodinuclear Compounds. *Inorg. Chem.* **2015**, *54*, 10316−10322.
(33) Tangoulis, V.; Nastopoulos, V.; Panagiotou, N.; Tasiopoulos, A.; Itskos, G.; Athanasiou, M.; Moreno-Pineda, E.; Wernsdorfer, W.; Schulze, M.; Malina, O. High-Performance Luminescence Thermometer with Field-Induced Slow Magnetic Relaxation Based on a Heterometallic Cyanido-Bridged 3d-4f Complex. *Inorg. Chem.* **2022**, *61*, 2546−2557.
(34) Petrosyants, S. P.; Ilyukhin, A. B.; Efimov, N. N.; Gavrikov, A. V.; Novotortsev, V. M. Self-Assembly and SMM Properties of Lanthanide Cyanocobaltate Chain Complexes with Terpyridine as Blocking Ligand. *Inorg. Chim. Acta* **2018**, *482*, 813−820.
(35) Chorazy, S.; Wang, J.; Ohkoshi, S. I. Yellow to Greenish-Blue Colour-Tunable Photoluminescence and 4f-Centered Slow Magnetic Relaxation in a Cyanido-Bridged DyIII(4-Hydroxypyridine)-CoIII Layered Material. *Chem. Commun.* **2016**, *52*, 10795−10798.
(36) Xin, Y.; Wang, J. H.; Zychowicz, M.; Zakrzewski, J. J.; Nakabayashi, K.; Sieklucka, B.; Chorazy, S.; Ohkoshi, S. Dehydration-Hydration Switching of Single-Molecule Magnet Behavior and Visible Photoluminescence in a Cyanido-Bridged (DyCoIII)-Co-III Framework. *J. Am. Chem. Soc.* **2019**, *141*, 18211−18220.
(37) *CrysAlisPRO, version 1.171.38.43*; Rigaku Oxford Diffraction Ltd.: Yarnton, U.K., 2015.
(38) Altomare, A.; Cascarano, G.; Giacovazzo, C.; Guagliardi, A.; Burla, M. C.; Polidori, G.; Camalli, M. SIR 92 − a Program for Automatic Solution of Crystal Structures by Direct Methods. *J. Appl. Crystallogr.* **1994**, *27*, 435.
(39) Sheldrick, G. M. Crystal Structure Refinement with SHELXL. *Acta Crystallogr., Sect. C* **2015**, *71*, 3−8.
(40) Spek, A. L. PLATON SQUEEZE: A Tool for the Calculation of the Disordered Solvent Contribution to the Calculated Structure Factors. *Acta Crystallogr., Sect. C* **2015**, *71*, 9−18.
(41) Spek, A. L. Structure Validation in Chemical Crystallography. *Acta Crystallogr., Sect. D* **2009**, *65*, 148−155.
(42) Farrugia, L. J. WinGX and ORTEP for Windows: An Update. *J. Appl. Crystallogr.* **2012**, *45*, 849−854.
(43) Brandenburg, K.*DIAMOND: Program for Crystal and Molecular Structure Visualization*; Crystal Impact GbR: Bonn, Germany, 2014.
(44) Macrae, C. F.; Sovago, I.; Cottrell, S. J.; Galek, P. T. A.; McCabe, P.; Pidcock, E.; Platings, M.; Shields, G. P.; Stevens, J. S.; Towler, M.; Wood, P. A. Mercury 4.0: From Visualization to Analysis, Design and Prediction. *J. Appl. Crystallogr.* **2020**, *53*, 226−235.
(45) Pilichos, E.; Spanakis, E.; Maniaki, E.-K.; Raptopoulou, C. P.; Psycharis, V.; Turnbull, M. M.; Perlepes, S. P. Diversity of Coordination Modes in a Flexible Ditopic Ligand Containing 2-Pyridyl, Carbonyl and Hydrazone Functionalities: Mononuclear and Dinuclear Cobalt(III) Complexes, and Tetranuclear Copper(II) and Nickel(II) Clusters. *Magnetochemistry* **2019**, *5*, 39.
(46) Eliseeva, S. V.; Pleshkov, D. N.; Lyssenko, K. A.; Lepnev, L. S.; Bünzli, J.-C. G.; Kuzmina, N. P. Deciphering Three Beneficial Effects of 2,2′-Bipyridine- N, N′-Dioxide on the Luminescence Sensitization of Lanthanide(III) Hexafluoroacetylacetonate Ternary Complexes. *Inorg. Chem.* **2011**, *50*, 5137−5144.
(47) Tanase, S.; Andruh, M.; Müller, A.; Schmidtmann, M.; Mathonière, C.; Rombaut, G. Construction of 3d−4f Heterometallic Coordination Polymers by Simultaneous Use of Hexacyanometalate Building-Blocks and Exo-Bidentate Ligands. *Chem. Commun.* **2001**, 1084−1085.
(48) Miquel, L.; Casanova, J.; Girera, J.; Alemany, P.et al.*SHAPE 2.1: Program for the Stereochemical Analysis of Molecular Fragments by Means of Continuous Shape Measures and Associated Tools*; University of Barcelona: Barcelona, 2013.
(49) Kepert, D. L.*Inorganic Stereochemistry*; Springer-Verlag: New York, 1982.
(50) Liu, J.; Reta, D.; Cleghorn, J. A.; Yeoh, Y. X.; Ortu, F.; Goodwin, C. A. P.; Chilton, N. F.; Mills, D. P. Light Lanthanide Metallocenium Cations Exhibiting Weak Equatorial Anion Interactions. *Chem. − Eur. J.* **2019**, *25*, 7749−7758.
(51) Chen, Y.-C.; Huang, X.-S.; Liu, J.-L.; Tong, M.-L. Magnetic Dynamics of a Neodymium(III) Single-Ion Magnet. *Inorg. Chem.* **2018**, *57*, 11782−11787.
(52) Pan, Y. Z.; Hua, Q. Y.; Lin, L. S.; Qiu, Y. B.; Liu, J. L.; Zhou, A. J.; Lin, W. Q.; Leng, J. D. A Slowly Magnetic Relaxing Sm^{III} monomer with a: D_{5h} equatorial Compressed Ligand Field. *Inorg. Chem. Front.* **2020**, *7*, 2335−2342.
(53) Shrivastava, K. N. Theory of Spin−Lattice Relaxation. *Phys. Status Solidi B* **1983**, *117*, 437−458.
(54) McGlynn, E. Electron Paramagnetic Resonance of Transition Ions, Oxford Classic Texts in the Physical Sciences, by A. Abragam and B. Bleaney. *Contemp. Phys.* **2013**, *54*, 115−116.
(55) Wernsdorfer, W.; Chakov, N. E.; Christou, G. Determination of the Magnetic Anisotropy Axes of Single-Molecule Magnets. *Phys. Rev. B* **2004**, *70*, No. 132413.
(56) Wernsdorfer, W. From Micro- to Nano-SQUIDs: Applications to Nanomagnetism. *Supercond. Sci. Technol.* **2009**, *22*, No. 064013.

(57) Moreno-Pineda, E.; Taran, G.; Wernsdorfer, W.; Ruben, M. Quantum Tunnelling of the Magnetisation in Single-Molecule Magnet Isotopologue Dimers. *Chem. Sci.* **2019**, *10*, 5138−5145.
(58) Galván, I. F.; Vacher, M.; Alavi, A.; Angeli, C.; Aquilante, F.; Autschbach, J.; Bao, J. J.; Bokarev, S. I.; Bogdanov, N. A.; Carlson, R. K.; Chibotaru, L. F.; Creutzberg, J.; Dattani, N.; Delcey, M. G.; Dong, S. S.; Dreuw, A.; Freitag, L.; Frutos, L. M.; Gagliardi, L.; Gendron, F.; Giussani, A.; González, L.; Grell, G.; Guo, M.; Hoyer, C. E.; Johansson, M.; Keller, S.; Knecht, S.; Kovačević, G.; Källman, E.; Li Manni, G.; Lundberg, M.; Ma, Y.; Mai, S.; Malhado, J. P.; Malmqvist, PÅ.; Marquetand, P.; Mewes, S. A.; Norell, J.; Olivucci, M.; Oppel, M.; Phung, Q. M.; Pierloot, K.; Plasser, F.; Reiher, M.; Sand, A. M.; Schapiro, I.; Sharma, P.; Stein, C. J.; Sørensen, L. K.; Truhlar, D. G.; Ugandi, M.; Ungur, L.; Valentini, A.; Vancoillie, S.; Veryazov, V.; Weser, O.; Wesołowski, T. A.; Widmark, P.-O.; Wouters, S.; Zech, A.; Zobel, J. P.; Lindh, R. OpenMolcas: From Source Code to Insight. *J. Chem. Theory Comput.* **2019**, *15*, 5925−5964.
(59) Aquilante, F.; Autschbach, J.; Carlson, R. K.; Chibotaru, L. F.; Delcey, M. G.; De Vico, L.; Galván, I.; Ferré, N.; Frutos, L. M.; Gagliardi, L.; Garavelli, M.; Giussani, A.; Hoyer, C. E.; Li Manni, G.; Lischka, H.; Ma, D.; Malmqvist, PÅ.; Müller, T.; Nenov, A.; Olivucci, M.; Pedersen, T. B.; Peng, D.; Plasser, F.; Pritchard, B.; Reiher, M.; Rivalta, I.; Schapiro, I.; Segarra-Martí, J.; Stenrup, M.; Truhlar, D. G.; Ungur, L.; Valentini, A.; Vancoillie, S.; Veryazov, V.; Vysotskiy, V. P.; Weingart, O.; Zapata, F.; Lindh, R. Molcas 8: New Capabilities for Multiconfigurational Quantum Chemical Calculations across the Periodic Table. *J. Comput. Chem.* **2016**, *37*, 506−541.
(60) Roos, B. O.; Lindh, R.; Malmqvist, P. Å.; Veryazov, V.; Widmark, P. O. Main Group Atoms and Dimers Studied with a New Relativistic ANO Basis Set. *J. Phys. Chem. A* **2004**, *108*, 2851−2858.
(61) Roos, B. O.; Lindh, R.; Malmqvist, P.-Å.; Veryazov, V.; Widmark, P.-O. New Relativistic ANO Basis Sets for Transition Metal Atoms. *J. Phys. Chem. A* **2005**, *109*, 6575−6579.
(62) Pineda, E. M.; Chilton, N. F.; Marx, R.; Dörfel, M.; Sells, D. O.; Neugebauer, P.; Jiang, S.-D.; Collison, D.; van Slageren, J.; McInnes, E. J, L.; Winpenny, R. E. P. Direct Measurement of Dysprosium(III)dysprosium(III) Interactions in a Single-Molecule Magnet. *Nat. Commun.* **2014**, *5*, No. 5243.
(63) Long, J.; Habib, F.; Lin, P. H.; Korobkov, I.; Enright, G.; Ungur, L.; Wernsdorfer, W.; Chibotaru, L. F.; Murugesu, M. Single-Molecule Magnet Behavior for an Antiferromagnetically Superexchange-Coupled Dinuclear Dysprosium(III) Complex. *J. Am. Chem. Soc.* **2011**, *133*, 5319−5328.
(64) Yu, W.; Schramm, F.; Pineda, E. M.; Lan, Y.; Fuhr, O.; Chen, J.; Isshiki, H.; Wernsdorfer, W.; Wulfhekel, W.; Ruben, M. Single-Molecule Magnet Behavior in 2,2′-Bipyrimidine-Bridged Dilanthanide Complexes. *Beilstein J. Nanotechnol.* **2016**, *7*, 126−137.
(65) Chilton, N. F.; Anderson, R. P.; Turner, L. D.; Soncini, A.; Murray, K. S. PHI: A Powerful New Program for the Analysis of Anisotropic Monomeric and Exchange-Coupled Polynuclear d- and f-Block Complexes. *J. Comput. Chem.* **2013**, *34*, 1164−1175.
(66) Lines, M. E. Orbital Angular Momentum in the Theory of Paramagnetic Clusters. *J. Chem. Phys.* **1971**, *55*, 2977−2984.
(67) (a) Das, C.; Upadhyay, A.; Vaidya, S.; Singh, S. K.; Rajaraman, G.; Shanmugam, M. Origin of SMM behaviour in an asymmetric Er(III) Schiff base complex: a combined experimental and theoretical study. *Chem. Commun.* **2015**, *51*, 6137−6140. (b) Qu, Y. X.; Ruan, Z. Y.; Huang, G. Z.; Chen, Y. C.; Liu, Y.; Jia, J. H.; Liu, J. L.; Tong, M. L. Sensitive magnetic-field-response magnetization dynamics in a one-dimensional dysprosium coordination polymer. *Inorg. Chem. Front.* **2021**, *8*, 4657−4665. (c) Pineda, E. M.; Chilton, N. F.; Tuna, F.; Winpenny, R. E. P.; McInnes, E. J. L. Systematic Study of a Family of Butterfly-Like {M(2)Ln(2)} Molecular Magnets (M = Mg^{-II}, Mn^{-II}, Co^{-II}, Ni^{-II}, and Cu^{-II}; Ln = Y^{-III}, Gd^{-III}, Tb^{-III}, Dy^{-III}, Ho^{-III}, and Er^{-III}). *Inorg. Chem.* **2015**, *54*, 5930−5941.
(68) Zhou, X.; Chen, L.; Jiang, S.; Xiang, G.; Li, L.; Tang, X.; Luo, X.; Pang, Y. Eu^{3+} Activated $LiSrVO_4$ Phosphors: Emission Color Tuning and Potential Application in Temperature Sensing. *Dyes Pigm.* **2018**, *151*, 219−226.
(69) Zhou, S.; Duan, C.; Yin, M.; Zhang, S.; Wang, C. High-Sensitive Optical Temperature Sensing Based on $^5D_1$ Emission of Eu^{3+} in YVO_4. *J. Alloys Compd.* **2019**, *784*, 970−974.
(70) Duan, D.; Wang, Y.; Jiang, S.; Li, L.; Xiang, G.; Tang, X.; Li, Y.; Zhou, X. An Optical Thermometry Based on Abnormal Negative Thermal Quenching of the Charge Transfer Band Edge. *J. Lumin.* **2019**, *215*, No. 116636.
(71) Kolesnikov, I. E.; Mamonova, D. V.; Kurochkin, M. A.; Kolesnikov, E. Y.; Lähderanta, E. Multimode Luminescence Thermometry Based on Emission and Excitation Spectra. *J. Lumin.* **2021**, *231*, No. 117828.
(72) de Souza, K. M. N.; Silva, R. N.; Silva, J. A. B.; Brites, C. D. S.; Francis, B.; Ferreira, R. A. S.; Carlos, L. D.; Longo, R. L. Novel and High-Sensitive Primary and Self-Referencing Thermometers Based on the Excitation Spectra of Lanthanide Ions. *Adv. Opt. Mater.* **2022**, *10*, No. 2200770.
(73) Brites, C. D. S.; Millán, A.; Carlos, L. D.*Lanthanides in Luminescent Thermometry*; Bünzli, J.-C. G.; Pecharsky, V. K., Eds.; Elsevier Science B.V: Amsterdam, 2016; Vol. *49*.
(74) Thompson, L. C.; Marvin, J. R.; Bettenberg, N. C. Absorption Spectra of Solid Rare Earth Complexes Obtained from the Inner Filter Effect on Luminescence. *J. Alloys Compd.* **1992**, *180*, 229−234.
(75) Molina, C.; Ferreira, R. A. S.; Poirier, G.; Fu, L.; Ribeiro, S. J. L.; Messsaddeq, Y.; Carlos, L. D. Er3+-Based Diureasil Organic-Inorganic Hybrids. *J. Phys. Chem. C* **2008**, *112*, 19346−19352.